Powerful radiative jets in supercritical accretion discs around non-spinning black holes

Aleksander Sądowski[1]⋆ and Ramesh Narayan[2]

[1]*MIT Kavli Institute for Astrophysics and Space Research, 77 Massachusetts Ave, Cambridge, MA 02139, USA*
[2]*Harvard-Smithsonian Center for Astrophysics, 60 Garden St., Cambridge, MA 02134, USA*

ABSTRACT

We describe a set of simulations of supercritical accretion on to a non-rotating supermassive black hole (BH). The accretion flow takes the form of a geometrically thick disc with twin low-density funnels around the rotation axis. For accretion rates $\gtrsim 10\,\dot{M}_{\rm Edd}$, there is sufficient gas in the funnel to make this region optically thick. Radiation from the disc first flows into the funnel, after which it accelerates the optically thick funnel gas along the axis. The resulting jet is baryon loaded and has a terminal density-weighted velocity $\approx 0.3c$. Much of the radiative luminosity is converted into kinetic energy by the time the escaping gas becomes optically thin. These jets are not powered by BH rotation or magnetic driving, but purely by radiation. Their characteristic beaming angle is ~ 0.2 rad. For an observer viewing down the axis, the isotropic equivalent luminosity of total energy is as much as $10^{48}\,{\rm erg\,s^{-1}}$ for a $10^7\,{\rm M}_\odot$ BH accreting at 10^3 Eddington. Therefore, energetically, the simulated jets are consistent with observations of the most powerful tidal disruption events, e.g. Swift J1644. The jet velocity is, however, too low to match the Lorentz factor $\gamma > 2$ inferred in J1644. There is no such conflict in the case of other tidal disruption events. Since favourably oriented observers see isotropic equivalent luminosities that are highly super-Eddington, the simulated models can explain observations of ultraluminous X-ray sources, at least in terms of luminosity and energetics, without requiring intermediate-mass BHs.

Key words: accretion, accretion discs– black hole physics – relativistic processes – galaxies: jets – X-rays: individual: Sw J1644+57 – X-rays: individual: SS433 – X-rays: ULX.

1 INTRODUCTION

Accretion flows around compact objects are commonly associated with relativistic jets. Such jets in active galactic nuclei, X-ray binaries in the low/hard state and gamma-ray bursts can be extremely powerful and can reach high Lorentz factors. It is believed that jets are driven by the rotational energy of a spinning black hole (BH) extracted via magnetic fields (Blandford & Znajek 1977, hereafter BZ). The efficiency of energy extraction depends on the BH spin and the magnetic flux threading the BH horizon. The maximal power for a given spin is reached when the magnetic flux saturates at the value characteristic of the magnetically arrested disc (MAD) state (Igumenshchev, Narayan & Abramowicz 2003; Narayan, Igumenshchev & Abramowicz 2003; Tchekhovskoy, Narayan & McKinney 2011; McKinney, Tchekhovskoy & Blandford 2012), i.e. when the magnetic pressure near the horizon on average balances the ram pressure of the accretion flow. For rapidly rotating BHs, the power of rela-

tivistic jets in the MAD state can exceed $\dot{M}c^2$ (Tchekhovskoy et al. 2011; Tchekhovskoy & McKinney 2012), i.e. more energy can go into the jet than the entire rest mass energy accreted by the BH. Such relativistic and magnetic jets have been extensively studied in recent years, both numerically (e.g. Tchekhovskoy, Narayan & McKinney 2010; Tchekhovskoy et al. 2011; Tchekhovskoy & McKinney 2012) and analytically (e.g. Penna, Narayan & Sądowski 2013a; Lasota et al. 2014). Although these studies have focused predominantly on hot, optically thin, geometrically thick accretion flows, recent numerical simulations (McKinney et al. 2014; Sądowski et al. 2014) suggest that BH rotation-driven jets may be produced with comparable efficiency even in the case of optically thick accretion flows.

Relativistic jets are often invoked to explain the observed X-ray luminosities of tidal disruption events (TDEs). When a star is disrupted by a supermassive BH, part of the debris returns to the BH and is accreted at a very high, significantly super-Eddington ('super-critical') mass accretion rate. The isotropic equivalent X-ray emission can reach as much as $10^{48}\,{\rm erg\,s^{-1}}$ (Bloom et al. 2011; Burrows et al. 2011). It is believed that this radiation is produced in internal shocks within a relativistic jet. However, as mentioned

Table 1. Model parameters.

Name	$\mathcal{K}$	ρ_{max} (g cm^{-3})	t_{max} (GM/c^3)	$\langle \dot{M} \rangle / \dot{M}_{\mathrm{Edd}}$	η (per cent)
A	10.0	5.95×10^{-7}	200 000	45	5.3
B	5.0	4.76×10^{-6}	170 000	310	4.0
C	1.0	5.95×10^{-4}	190 000	4800	4.6

Notes. $\mathcal{K} = p/\rho^{\Gamma}$ is the initial torus entropy parameter (see Penna et al. 2013b) and is given in $G = c = 1$ units. ρ_{max} is the corresponding maximal density of the initial torus. Other parameters: BH mass: $M_{\mathrm{BH}} = 3 \times 10^5$ M$_{\odot}$, non-dimensional BH spin parameter: $a_* \equiv a/M = 0.0$, resolution: 304×192, radial extent of the domain: $R_{\mathrm{min}} = 1.85$ to $R_{\mathrm{max}} = 10\,000$, grid parameters (defined in Sądowski et al. 2015) $R_0 = 1.0$, $H_0 = 0.6$, minimal initial ratio of magnetic to total pressures: $\beta_{\mathrm{max}} = 10.0$.

above, the most powerful jets require accumulation of a significant amount of magnetic flux, and the disrupted star is incapable of providing this flux (Tchekhovskoy et al. 2014). In addition, a rapidly spinning BH is required to produce an effective BZ jet.

The initial mass accretion rate in a TDE is super-Eddington, which is very different from the highly sub-Eddington, radiatively inefficient regime that is usually considered when studying magnetic jets. A super-Eddington accretion disc is dominated by radiation pressure and the gas is optically thick. It was predicted already by Paczyński & Wiita (1980) that such discs will be superluminous. What is more, the large thickness of the disc naturally collimates radiation along the rotation axis, producing a significantly super-Eddington flux of energy in the funnel (Sikora 1981; Narayan, Nityananda & Wiita 1983) which can accelerate gas to mildly relativistic velocities (Sikora & Wilson 1981). Such radiatively driven jets should occur in any supercritical accretion flow and should be present even if the BH is non-rotating or if there is little magnetic flux threading the BH horizon. In this work, we study in detail the properties of such purely radiative (non-BZ) jets by means of general relativistic (GR) radiation magnetohydrodynamic (MHD) simulations.

The paper is organized as follows. In Section 2, we describe the numerical method. In Section 3, we present the results, and discuss in detail the location of the photosphere (Section 3.1), the properties of the radiative jet (Section 3.2), the corresponding luminosities (Section 3.3) and the beaming factor (Section 3.4). In Section 4, we discuss applications to TDEs, ultraluminous X-ray sources (ULXs) and SS433.

2 NUMERICAL METHODS

We performed a set of three simulations of super-Eddington accretion on a non-rotating, $a_* = 0$, moderately supermassive, $M_{\mathrm{BH}} = 3 \times 10^5$ M$_{\odot}$, BH. We used the GR radiation magnetohydrodynamical (RMHD) code KORAL (Sądowski et al. 2013a, 2014), which evolves gas and magnetic field in the ideal MHD approximation, together with the radiation field under the M1 closure scheme (Levermore 1984). The models were initialized as optically thick equilibrium tori of gas and radiation in local thermal equilibrium, threaded by multiple loops of weak magnetic field. The only difference in the initial states of the three simulations was the torus entropy parameter $\mathcal{K} = p/\rho^{\Gamma}$ (see Penna, Kulkarni & Narayan 2013b), which determines the initial torus density and thereby the mass accretion rate.

The simulations were axisymmetric and were run with a resolution of 304×192 cells in radius and polar angle, with polar cells concentrated towards the equatorial plane. Each simulation was evolved for an exceptionally long time – roughly 2000 orbital times at the innermost stable circular orbit. This was possible be-

cause the poloidal magnetic field was amplified and maintained at a physically reasonable level by means of a mean-field dynamo, as described in Sądowski et al. (2015). (Without the dynamo, the poloidal magnetic field would quickly decay because of axisymmetry of these 2D simulations. On the other hand, without restricting ourselves to 2D, it would be virtually impossible to run the simulations for such long durations.) The duration of the simulations was sufficiently long for the jet to reach equilibrium at the outer boundary of the grid, located at $r = 10\,000$.[1] We used the following formulae for the absorption and scattering opacities, κ_{abs} and κ_{es}, respectively,

$$\kappa_{\mathrm{abs}} = 6.4 \times 10^{22} \rho T^{-7/2} \, \mathrm{cm}^2 \, \mathrm{g}^{-1}, \qquad (1)$$

$$\kappa_{\mathrm{es}} = 0.34 \, \mathrm{cm}^2 \, \mathrm{g}^{-1}, \qquad (2)$$

where ρ and T are, respectively, the gas density and temperature in cgs units. The model parameters of the three simulations are given in Table 1 and are defined as in Sądowski et al. (2015).

The average accretion rates for models A, B and C were 45, 310 and 4800 $\dot{M}_{\mathrm{Edd}}$, respectively, where the critical accretion rate $\dot{M}_{\mathrm{Edd}}$ is defined as

$$\dot{M}_{\mathrm{Edd}} = \frac{L_{\mathrm{Edd}}}{\eta_0 c^2} = 2.44 \times 10^{18} \frac{M}{\mathrm{M}_{\odot}} \, \mathrm{g} \, \mathrm{s}^{-1}, \qquad (3)$$

where $L_{\mathrm{Edd}} = 1.25 \times 10^{38} \, M/\mathrm{M}_{\odot}$ erg s^{-1} is the Eddington luminosity, and η_0 is the radiative efficiency of a thin disc for zero BH spin: $\eta_0 = 0.057$. For the chosen BH mass ($M_{\mathrm{BH}} = 3 \times 10^5$ M$_{\odot}$), $L_{\mathrm{Edd}} = 3.75 \times 10^{43}$ erg s^{-1} and $\dot{M}_{\mathrm{Edd}} = 7.32 \times 10^{23}$ g s^{-1}.

Given the long durations of the runs (Table 1), the simulations reached inflow/outflow equilibrium[2] up to radius $r_{\mathrm{eq}} \sim 50$ in the bulk of the disc, where the gas moves inwards on average with a relatively low viscosity-driven velocity. In the region near the axis, where the gas flows out with quasi-relativistic velocities (as will be discussed below), the converged region extends out to the outer boundary at $r = 10\,000$.

3 RESULTS

3.1 Photosphere

The simulated accretion flows are characterized by high, supercritical accretion rates and form geometrically thick discs (as expected). Fig. 1 shows the time-averaged gas distribution in model A, with colour intensity indicating the mean density. Within the

---

[1] Throughout the paper, we adopt GM/c^2 as the unit of length, and GM/c^3 as the unit of time.

[2] Defined as a region where the local average radial velocity v^r satisfies $|v^r| > r/2t$ for a simulation of duration t.
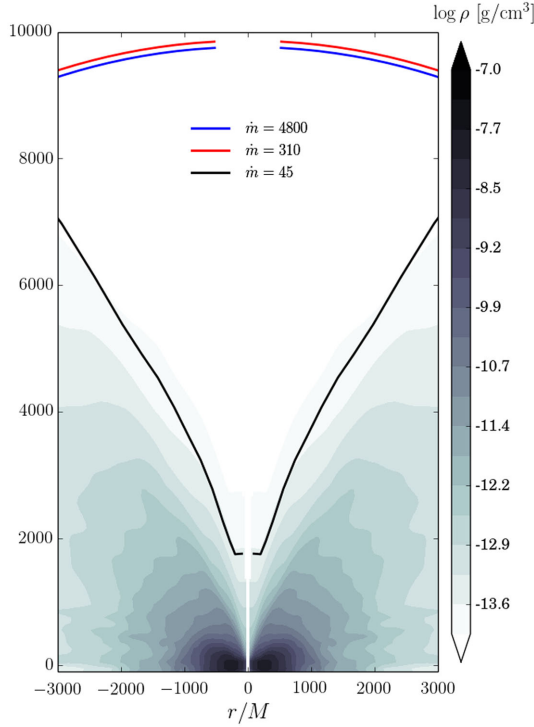
Figure 1. Photosphere profiles for models A (black), B (red) and C (blue lines). Only model A has its photosphere inside the computational domain. The other two lines represent only the formal location of the photosphere which coincides with the domain boundary at $r = 10\,000$. The colour levels represent the logarithm of density for model A.

inflow/outflow equilibrium radius ($r_{eq} \sim 50$) the disc density scale-height corresponds to $h/r \sim 0.3$, a typical value for supercritical and radiatively inefficient accretion flows. Although most of the gas is concentrated near the equatorial plane, a significant amount is blown away to form the wind region visible in Fig. 1 at intermediate polar angles. The lowest gas density is found near the polar axis. For model A (accreting at the lowest rate, $\dot{M} = 45\,\dot{M}_{Edd}$), the density on the axis at radius $r = 1000$ equals roughly $10^{-13}\,\mathrm{g\,cm^{-3}}$. This corresponds to an optical depth against scattering greater than unity over the distance $d = 1000 \approx 10^{13}\,\mathrm{cm}$. Thus, a significant fraction of the polar region is optically thick.

We estimate the radius of the photosphere in the funnel as a function of polar angle θ by integrating the optical depth from the outer boundary of the simulation box down towards the BH along fixed θ. In computing the optical depth, we allow for relativistic effects and follow the formalism given in Sądowski et al. (2015, their equations 47–49). The black contours in Fig. 1 show the location of the photosphere for model A. Even for this moderately supercritical model, the photosphere at the axis is located as far out as $r = 2000$. For larger accretion rates, the photosphere moves even farther out. In fact, for models B and C, it is formally located at the computational box boundary (red and blue lines in Fig. 1) which provides only a lower limit for the location of the actual photosphere.

3.2 Radiative jet

The left-hand panel of Fig. 2 shows again the density distribution in model A, but limited now to the inner regions and with gas velocity vectors superimposed. The right-hand panel shows the magnitude and direction of the energy flux. To explain the quantity that is
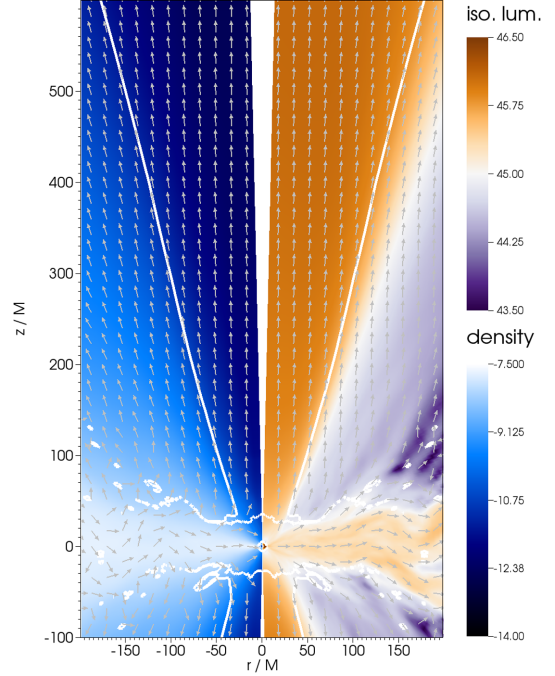

Figure 2. Time-averaged results for model A in the poloidal plane. Left-hand panel: colour shows the distribution of the logarithm of density (in $\mathrm{g\,cm^{-3}}$) and arrows show the gas velocity. The white contour shows the formal border of the jet region. Right-hand panel: colour shows the logarithm of isotropic equivalent luminosity of total energy (in $\mathrm{erg\,s^{-1}}$, for definition see equation 5) and arrows show the direction of the energy flux. The white contour shows the border.

plotted, we start with the stress–energy tensors, T_ν^μ, R_ν^μ, of the magnetized gas and radiation, and note that $-(T_t^r + R_t^r)$ at any point is the radial flux of total energy (gas, magnetic and radiation) at that point as measured by an observer at infinity (lab frame). Also, ρu^r, where ρ is the gas density in the fluid frame and u^r is the fluid four velocity in the lab frame, is the radial flux of rest mass energy. Thus,

$$F^r = -\left(T_t^r + R_t^r + \rho u^r\right) \tag{4}$$

describes the flux of 'useful energy' (i.e. rest mass energy subtracted out) as measured at infinity. Multiplying F^r by $4\pi r^2$ then gives the equivalent isotropic luminosity ($\mathrm{erg\,s^{-1}}$) that one infers from the measured flux at the given location,

$$L_{iso} = 4\pi r^2 F^r = -4\pi r^2 \left(T_t^r + R_t^r + \rho u^r\right). \tag{5}$$

The colours in the right-hand panel of Fig. 2 show this quantity, L_{iso}, as a function of position, with arrows indicating the direction of the energy flux in the poloidal plane.[3] Over the entire volume, energy flows out, i.e. $L_{iso} > 0$. In the region of the disc, bound gas is accreted, while in the wind and jet regions, unbound gas is ejected. Both correspond to positive L_{iso}. The highest energy flux is in the region near the polar axis. Interestingly, even for the relatively low accretion rate of $45\,\dot{M}_{Edd}$ in model A, the isotropic luminosity reaches $5 \times 10^{45}\,\mathrm{erg\,s^{-1}} \approx 130\,L_{Edd}$.

---

[3] The direction in the poloidal plane is determined by the vector $(\hat{F}^r, \hat{F}^\theta)$ built from orthonormal radial and polar components of the energy flux as defined in equation (4).
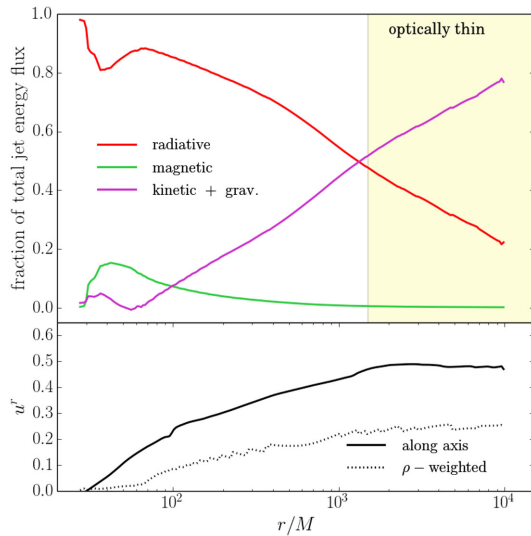
Figure 3. Top panel: fractional contribution in model A of radiative (R_t^r), magnetic ($b^2 u^r u_t - b^r b_t$) and kinetic plus gravitational ($\rho u^r u_t + \rho u^r$) components of the energy flux to the total flux in the jet region as a function of distance. The shaded zone corresponds to the optically thin region above the photosphere. Bottom panel: radial profiles of gas velocity in the jet region in model A. The solid line shows the gas velocity in the cell nearest to the axis, while the dotted line shows the density-weighted average velocity in the jet region.

To define the region corresponding to the jet, we follow Sądowski et al. (2013b) and require the local Bernoulli parameter μ, defined as

$$\mu = \frac{F^r}{\rho u^r} = -\frac{T_t^r + R_t^r + \rho u^r}{\rho u^r}, \tag{6}$$

to exceed 0.05, which corresponds to the velocity at infinity exceeding roughly 30 per cent of the speed of light. This definition is not fundamental for our analysis, but is useful when talking about averaged or integrated quantities in the funnel.

The white contour in Fig. 2 denotes the border of the jet region defined according to the criterion given above. The jet region coincides with the region of lowest density ($\rho \lesssim 10^{-10}$ g cm^{-3}, shown in the left-hand panel) as well as the region of highest energy flux ($L_{iso} \gtrsim 10^{45}$ erg s^{-1}, right-hand panel).

The top panel of Fig. 3 shows radial profiles of the fractional contributions of various components of the energy flux integrated over solid angle within the jet region. Red, purple and green lines correspond to the fluxes of radiative, kinetic and magnetic energies, respectively. The flux of thermal energy is negligible and is not shown.

In the region of the jet closest to the BH ($r \lesssim 1000$), the energy flux is dominated by radiation which comes from the innermost and hottest part of the disc. However, the relative contribution of the radiative flux decreases with increasing distance from the BH as radiative energy is converted into kinetic energy (radiation pressure pushes the gas out). The magnetic contribution is unimportant at all radii. This is by construction because we specifically chose non-BZ-like conditions for these simulations – non-spinning BH, weak magnetic field well below the MAD limit.

The transfer of energy from radiation to gas causes the gas velocity to accelerate along the funnel, as seen in the bottom panel of Fig. 3. The gas at the axis reaches roughly 50 per cent of the speed of light at distance $r \sim 1000$. The density-weighted gas velocity in the funnel reaches only $\sim$35 per cent of the speed of light, reflect-
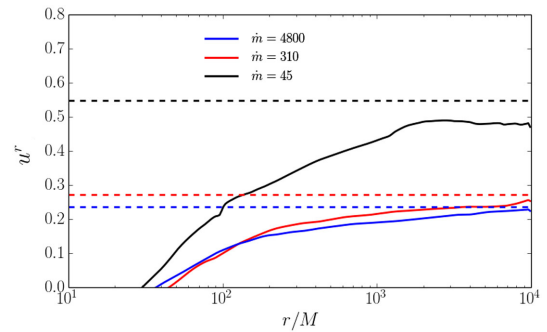

Figure 4. Radial velocity of the gas at the axis (solid lines) and the maximal velocity the gas will achieve if all the energy is converted into kinetic energy at infinity (dashed lines). Results are shown for all three models.

ing the fact that gas near the edge of the funnel is denser and less effectively accelerated.

Acceleration continues as long as momentum is transferred from the radiation, i.e. up to radius $r \approx 2000$. Constant gas velocity implies that the kinetic energy has saturated. However, the fractional contribution of the kinetic energy (purple line in the top panel) increases even further. This is because of the residual radiation crossing the borders of the jet region and increasing the kinetic contribution. Acceleration stops when radiation drag by photons from the funnel walls is large enough to counterbalance the acceleration by radiation flowing along the funnel (Sikora & Wilson 1981). In the framework of the M1 closure scheme, this corresponds to the situation where the gas comoves with the radiation rest frame, where no momentum is transferred between the radiation and the gas.

Even though we ran our simulations over a large domain extending to $r_{out} = 10\,000$, it turned out that the outer boundary was still not far enough out to resolve the photospheres of models B and C. In these models, gas acceleration occurs all the way to the boundary. Nevertheless, we can still estimate the terminal velocity of the gas by looking at the total energy flux near the boundary and assuming that all the energy is converted into kinetic energy at infinity. The velocities along the axis and the terminal velocities for the three models are shown in Fig. 4 by solid and dashed lines, respectively. The gas in the lowest accretion rate model A reaches saturated velocity $0.5c$ already at radius $r = 1000$. The terminal velocity for this model (black dashed line) is only $\sim$10 per cent higher, which means that almost all the available energy has been converted into kinetic energy. For the other two models, with accretion rates 310 and 4800 $\dot{M}_{Edd}$, the actual and terminal gas velocities are significantly lower and reach only 20–30 per cent of the speed of light. This is probably the result of more effective mass loading of the funnel region in these models. Because of the larger optical depth, we presume radiation more effectively drives gas towards the axis, which results in weaker acceleration of the gas in this region.

3.3 Luminosities

Fig. 5 presents the equivalent isotropic luminosity (top panel, equation 5) and the radial velocity of the gas (bottom panel) as a function of polar angle for models A ($\dot{M} = 45\ \dot{M}_{Edd}$), B (310 $\dot{M}_{Edd}$) and C (4800 $\dot{M}_{Edd}$). The luminosities were measured at radius $r = 5000$ and reflect the flux of total energy, which in the funnel/jet region is dominated by kinetic luminosity. The solid lines correspond to the region of the simulation domain where inflow/outflow equilibrium state has been reached at $r = 5000$. The dotted lines refer to
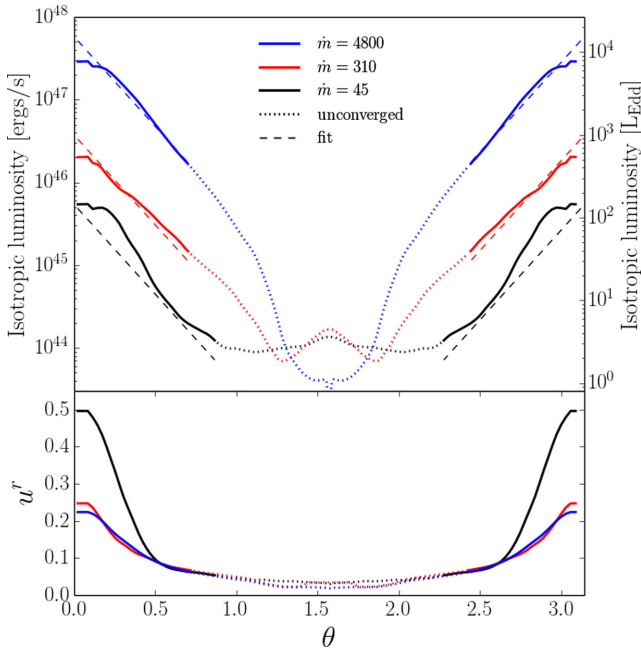
Figure 5. Top panel: isotropic equivalent luminosity (measured at $r = 5000$) for models A (black), B (red) and C (blue lines) as a function of the polar angle θ. The dashed lines show the fitting function given in equation (7) for a BH mass $M = 3 \times 10^5$ M$_\odot$. Bottom panel: velocity of the gas at $r = 5000$. In both panels, the solid lines correspond to the region of the simulation that is in inflow/outflow equilibrium at $r = 5000$, while the dotted lines refer to unconverged regions.

unconverged region, which is not in flow contact with the BH and therefore the results are less reliable.

For an observer looking precisely down the axis, $L_{iso} = 5 \times 10^{45}$ erg s^{-1} for model A, and increases to as much as 3×10^{47} erg s^{-1} for model C ($4800\dot{M}_{Edd}$). The isotropic equivalent luminosity is lower for off-axis observers, dropping by roughly an order of magnitude between the axis and the border of the jet region. The luminosities scale linearly with accretion rate, i.e. the efficiency of energy injection into the funnel region seems to be independent of the accretion rate.

The isotropic equivalent luminosity profiles are reasonably well described by the following fitting function,

$$L_{fit} = 4 \times 10^{47} e^{-\theta/\theta_{jet,0}} \frac{\dot{M}}{10^3 \dot{M}_{Edd}} \frac{M_{BH}}{10^6 \text{ M}_\odot}, \quad (7)$$

where the scaling with BH mass is included[4] and where $\theta_{jet,0} = 0.2$ is the characteristic jet beaming angle.[5]

The bottom panel of Fig. 5 shows the dependence of the gas velocity on polar angle for each of the models. Model A with the lowest accretion rate shows the most efficient acceleration. In all three models, the velocity quickly decreases with increasing θ and transitions to $u^r < 0.1$ in the wind region ($\theta > 0.5$).

---

[4] Although we simulated accretion flows on a supermassive BH (to directly show how strong the radiative jet can be), our results can be applied to any astrophysical BH by scaling them properly with mass. This is because the optical depth over given number of gravitational radii, which determines, e.g. the efficiency of gas/radiation interaction, is independent of BH mass for fixed fraction of Eddington accretion rate.

[5] Allowing for the fact that there is more solid angle at larger θ, a better estimate of the luminosity beaming angle is twice this: $\theta_{jet} \approx 0.4$.
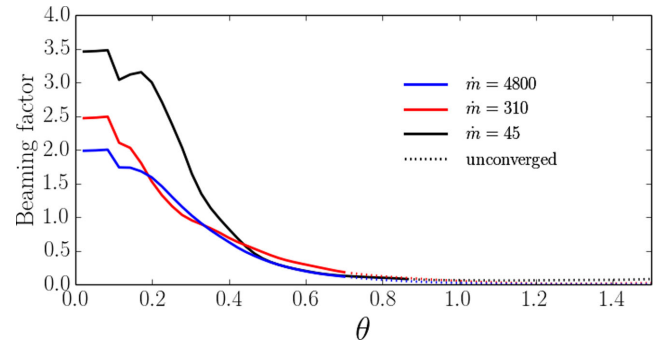

Figure 6. Beaming factor (for definition see equation 8) as a function of polar angle in the three simulations.

3.4 Beaming factor

Discs accreting at supercritical rates are geometrically very thick. As a result, energy in general and photons in particular escape preferentially along the axis, where the density and optical depth are lowest. Most of the energy escapes through the funnel, and the flux of energy decreases steeply with increasing polar angle (equation 7, Fig. 5). It is useful to define the beaming factor $b(\theta)$, which gives the ratio of the isotropic equivalent luminosity L_{iso} (defined in equation 5) inferred by an observer at polar angle θ to the real luminosity of the source L_{tot},

$$b = \frac{L_{iso}}{L_{tot}} = \frac{L_{iso}}{\eta \dot{M} c^2}, \quad (8)$$

where L_{tot} is obtained by integrating the energy flux over the sphere,[6]

$$L_{tot} = \int F^r \sqrt{-g} \, d\theta d\phi \equiv \eta \dot{M} c^2, \quad (9)$$

with η being the total efficiency of the accretion flow (results given in Table 1). When integrated over the sphere, the beaming factor should, on average, be equal to unity. However, because the equilibrium region at $r = 5000$ is limited to the polar region (gas near the equatorial plane was not able to relax yet because of long viscous time-scale there), this integral cannot be directly calculated.

Fig. 6 shows the beaming factor as a function of θ, as measured at radius $r = 5000$. For all three runs, b is maximum at the axis and decreases away from the axis. The maximal beaming factor is $b = 3.5$ for model A, and $b = 2.0$–2.5 for models B and C. More pronounced beaming in model A may come from the fact that, in this case, b is measured outside the photosphere. The beaming factor equals unity, i.e. local isotropic equivalent luminosity is equal to the true luminosity, at $\theta \approx 0.35$, which roughly coincides with the edge of the funnel. In the wind and disc regions, $b(\theta) \ll 1$, reflecting the fact that comparable amounts of energy leave in the funnel and in these regions, but the solid angle covered by the funnel is a small fraction of the whole sphere.

It should be emphasized that we defined the beaming factor $b(\theta)$ with respect to the *total luminosity* of the accretion flow, not the Eddington luminosity. The three simulations discussed in this paper are all energetically efficient, as reflected by the fact that they have efficiencies η (Table 1) nearly equal to the standard Novikov–Thorne thin disc efficiency, $\eta_0 = 0.057$. Correspondingly,

---

[6] In steady state, the integrated energy flux is independent of radius, so it can be evaluated at any convenient radius. The values of L_{tot} and η quoted here correspond to $r = 5000$.

$L_{\text{tot}}/L_{\text{Edd}} \approx \dot{M}/\dot{M}_{\text{Edd}}$. Therefore, if we define an Eddington-scaled beaming factor $b_{\text{Edd}}(\theta)$, we roughly expect

$$b_{\text{Edd}} \equiv \frac{L_{\text{iso}}}{L_{\text{Edd}}} \approx \frac{\dot{M}}{\dot{M}_{\text{Edd}}} b. \qquad (10)$$

Considering that b itself is of order a few along the axis, it is clear that b_{Edd} can be extremely large for highly super-Eddington accretion flows. If the BH was spinning and if it was threaded by a MAD-level magnetic field, the luminosity would be larger still by possibly a factor of several.

4 DISCUSSION

Magnetically dominated, BH rotation-powered jets in radiatively inefficient hot accretion flows have been simulated and studied now for a number of years. These jets operate through the BZ mechanism, in which ordered magnetic fields are twisted by the rotating BH. The twisted field lines unwind and expand in a direction parallel to the BH spin axis because of the collimating action of the geometrically thick accretion disc.

The jets studied in this paper involve different physics. Our BHs do not rotate and there is no strong ordered magnetic field,[7] so there is no opportunity for the BZ mechanism to operate. Nevertheless, the super-Eddington accretion flows considered here do produce powerful jets. Because these accretion discs are geometrically thick, they naturally form funnels oriented parallel to the angular momentum axis of the accretion flow (just as in the case of radiatively inefficient hot accretion flows). MRI-driven turbulence in the disc leads to energy dissipation in the disc interior,[8] which heats the gas. The gas, in turn, cools by emitting radiation. The radiation then flows down the gradient of density/optical depth via diffusion and turbulent transport (Jiang, Stone & Davis 2014), which naturally concentrates a significant amount of energy in the funnel region. There, radiation pressure accelerates gas outwards along the axis of the funnel, resulting in a jet that travels at a modest fraction (0.2–0.5) of the speed of light.

The process described above will take place so long as the accretion flow forms a thick disc with a funnel. Independently of whether the funnel is optically thin or thick, radiation always moves towards the axis.[9] Once there, it collimates and rushes out along the axis, transferring its momentum to the gas. The transfer operates as long as there is enough optical depth. Once the radiation crosses the photosphere, where radiative and kinetic energies are of the same order (see Fig. 3), the acceleration of the gas terminates.

Efficient conversion of radiative to kinetic energy happens only if there is sufficient optical depth along the funnel. Already for an accretion rate of 45 $\dot{M}_{\text{Edd}}$ (model A, the lowest $\dot{M}$ we have considered), most of the radiative energy is converted to kinetic energy. For lower accretion rates, the optical depth in the funnel will be
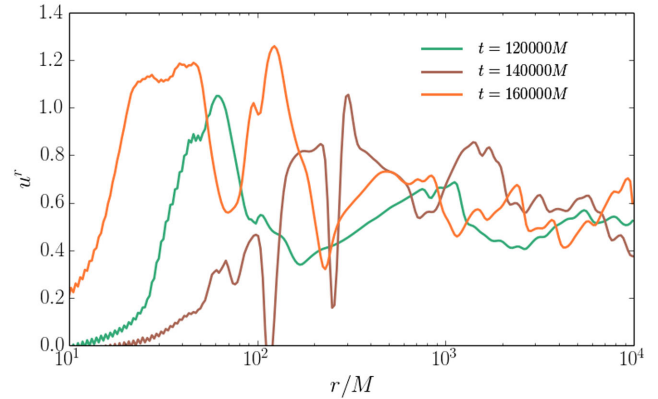
---

[7] The magnetic field is initiated as a series of oppositely polarized loops which when accreted cancel each other and prevent accumulation of significant magnetic flux at the BH horizon.

[8] In ideal MHD codes like ours this dissipation takes place on a grid scale. Because the code conserves energy perfectly, the lost energy automatically comes back as gas entropy.

[9] In the case of an optically thin funnel, there is a photosphere which is significantly inclined to the equatorial plane and which by itself forms a conical emitting surface. Radiation coming from this surface will be naturally emitted towards the axis and will fill the funnel region. If the funnel is optically thick, then radiation will flow down the gradient of the radiative energy density which is again towards the axis.

Figure 7. Velocity profiles along the axis for model A corresponding to three epochs.

lower, and we expect that a larger fraction of the jet energy will remain in the form of radiation rather than gas kinetic energy. However, the total jet power should scale similarly for all supercritical accretion rates. This is because the efficiency of accretion and the thickness of the disc (which collimates the jet) are independent of the accretion rate in this regime (Sądowski et al. 2015).

Can the kinetic energy escaping the funnel be observed by a distant observer? Yes, provided it is converted back into radiation. In magnetic jets, reconnection is possibly a dominant mechanism for this conversion (Sironi, Petropoulou & Giannios 2015). However, magnetic reconnection is unlikely to be important for the radiatively driven jets considered here since there is so little magnetic energy (Fig. 3). Shocks are a more natural mechanism for converting the gas kinetic energy to radiation via non-thermal particle acceleration. To show that shocks are quite likely, Fig. 7 presents the radial profile of gas velocity near the axis for model A at three different moments of time. We see that the velocity profiles along the funnel are highly variable. Layers (shells) of gas moving with higher than average velocity will ultimately overtake preceding lower velocity gas, thereby producing shocks (especially in optically thin regions) outside our computational domain. Such "internal shocks" will dissipate a good fraction of the kinetic energy, converting it to thermal and non-thermal energy and ultimately into radiation. What fraction of the total energy flux measured at $r = 5000$ (Fig. 5) reaches the observer in the form of radiation depends on the geometry and dynamics of this process. The energy distribution of the reprocessed radiation can be significantly different from that of the original radiation in the funnel. Estimating the spectral shape is, however, beyond the scope of this paper.

4.1 Comparison with previous works

Studies of geometrically thick discs corresponding to high accretion rates were initiated in the late 1970s by authors studying thick equilibrium torii (Fishbone & Moncrief 1976; Abramowicz, Jaroszynski & Sikora 1978; Kozlowski, Jaroszynski & Abramowicz 1978; Jaroszynski, Abramowicz & Paczynski 1980). It was realized that if torii are thick and radiative pressure supported, their total luminosity must exceed the Eddington limit (Paczyński & Wiita 1980). Later works by Sikora (1981), Sikora & Wilson (1981) and Narayan et al. (1983) specifically analysed the properties of the polar outflows. The accretion flows were modelled by thick equilibrium torii with arbitrarily prescribed angular momentum profiles. It was shown that, if such torii are thick enough, the local radiative

flux in the funnel may significantly exceed the Eddington value. Sikora & Wilson (1981) showed in addition that the flow cannot convert more than a small fraction of the disc's radiative luminosity into kinetic energy in the polar outflow because of radiation drag. However, the authors noted that the acceleration may be more efficient if the funnel is optically thick. These predictions are in perfect agreement with our study. Similar topics were studied in the past by Abramowicz & Piran (1980), Piran (1982) and Abramowicz, Ellis & Lanza (1990).

In Madau (1988), the author studied the dependence on viewing angle of the observed disc spectrum of geometrically and optically thick accretion discs around supermassive BHs in quasars and showed that the funnel dominates the emission from tori which are viewed at small inclination angles from the symmetry axis of the torus. Our study, based on numerical approach, confirms this result.

Numerical simulations of supercritical accretion are relatively new. The field was initiated in a series of seminal works by Ohsuga et al. (2005, 2009), and Ohsuga & Mineshige (2007, 2011), who performed radiation hydrodynamical, and later MHD simulations using a non-relativistic code and adopting the flux-limited diffusion approximation. More recently, our group developed GR numerical codes with M1 radiative closure and applied it to supercritical accretion (McKinney et al. 2014; Sądowski et al. 2014, 2015). A similar scheme was implemented in an independent radiation GRMHD code by Fragile, Olejar & Anninos (2014). Most recently, Jiang et al. (2014) simulated a supercritical accretion flow using a Newtonian code with cylindrical coordinates (and a cylindrical BH). The authors solved the radiative transfer equation directly on a fixed grid of angles, instead of applying any radiative closure.

All the studies cited above agree qualitatively on the main features of supercritical accretion, namely that there is no barrier to super-Eddington accretion, that these flows are optically and geometrically thick, and that they are characterized by strong polar outflows and significant winds. The detailed composition of the outflows differs between studies, e.g. in Jiang et al. (2014) energy flows out primarily via radiation, whereas our jets are kinetic energy dominated, and the reason for this is presently unclear. Our work is the first one to study polar outflows using a GR code. Also, we simulated accretion on to a (mildly) supermassive BH (all previous work considered stellar-mass BHs).

In a work similar to ours, Takeuchi, Ohsuga & Mineshige (2010) studied radiatively driven jets using a Newtonian code and simulated an accretion flow with $\dot{M} \approx 6\,\dot{M}_{\text{Edd}}$. The authors focused on the acceleration and collimation mechanisms of the radiative jet. They showed that the jet can be accelerated up to mildly relativistic speeds by the radiation-pressure force and collimated by the Lorentz force of a magnetic tower structure in the innermost region. They also pointed out the importance of the radiative drag force in limiting gas acceleration in Takahashi & Ohsuga (2015). The gas velocities they obtained are in perfect agreement with our study. However, we do not observe magnetic collimation of the outflow. This discrepancy may be related to the fact that the simulated flows in the present work have significantly higher accretion rates.

4.2 Astrophysical implications

A principal result of this paper is that supercritical accretion on BHs leads to a collimated outflow of energy along the polar axis even if the BH spin is zero and BZ-like extraction of BH rotational energy is ruled out. For observers looking directly down the funnel, the isotropic-equivalent luminosity can significantly exceed the Eddington luminosity (equation 7). The observed luminosity drops

with increasing polar angle. We discuss the importance of these results in the context of TDEs, ULXs and the microquasar SS433.

4.2.1 Tidal disruption events

Whenever a star comes closer to a supermassive BH than its tidal radius, it is disrupted by the tidal gravitational field (Rees 1988; Evans & Kochanek 1989). Approximately half the mass of the star remains bound to the BH and returns after a while to the vicinity of the BH. Relativistic precession causes the tidal stream to interact with itself, shock and circularize (e.g. Bonnerot et al. 2015; Shiokawa et al. 2015). Once the gas circularizes, it starts to build up magnetic field which triggers accretion. According to the standard model (e.g. Krolik & Piran 2012), for typical parameters (stellar mass star disrupted by a $\sim 10^6\,M_{\odot}$ BH), the peak accretion rate at the onset of accretion can exceed $10^3\,\dot{M}_{\text{Edd}}$. This accretion rate subsequently declines as $t^{-5/3}$.

In the case of the TDE Swift J1644, the observed isotropic-equivalent X-ray luminosity was as high as $10^{48}\,\text{erg s}^{-1}$ during the initial outburst peak (Bloom et al. 2011; Burrows et al. 2011). This fact, together with the properties of the radio emission, led to the suggestion that the extreme luminosity was produced by a relativistic jet driven by rotational energy of the BH. However, efficient extraction of BH spin energy requires the accumulation of significant magnetic flux at the BH, far more than the disrupted star can provide (Tchekhovskoy et al. 2014). This problem could be overcome if the tidal stream is able to drag magnetic field from a pre-existing accretion flow around the BH (Kelley, Tchekhovskoy & Narayan 2014).

The initial highly super-Eddington regime of accretion in a TDE corresponds precisely to the simulations discussed in this study, where we consider supercritical accretion on a supermassive BH with $\dot{M}$ of order tens to thousands of Eddington. We can therefore explore whether a purely radiative jet, similar to the ones studied in this work, can explain observations of TDE jets. As shown in Section 3.3, for an observer looking down the funnel, the isotropic equivalent luminosity reaches (equation 7) $10^{47}\,\text{erg s}^{-1}$ for canonical TDE parameters. By increasing the BH mass by an order of magnitude to $10^7\,M_{\odot}$, it is possible to match the peak luminosity observed in Swift J1644. However, the radio emission in the afterglow of this TDE event suggests that the jet must have been relativistic, with Lorentz factor $\gtrsim 2$ (Berger et al. 2012). Such high velocities are difficult with purely radiative acceleration – the radiation field in the funnel is not sufficiently collimated, and acceleration is prevented by radiative drag. Therefore, it seems that radiative jets alone cannot explain the properties of Swift J1644. Instead, the jet in this object probably involved a combination of radiatively and BH rotational energy-driven acceleration.

Some other TDE candidate events, e.g. PS1-10jh (Gezari et al. 2012), PS1-11af (Chornock et al. 2014) and PTF09ge (Arcavi et al. 2014), did not show significant X-ray and radio emission, but were observed in the ultraviolet band only. This fact may be explained if we assume that these sources do not produce strong magnetic jets accelerating gas to such high velocities as in the case of Swift J1644. Having in mind that the onset of accretion of the returning debris corresponds to strongly supercritical accretion, and that the luminosities are super-Eddington, the observed optical emission would come from the funnel region where it is reprocessed through the kinetic flux, as discussed in this work. It could also come directly from the inner funnel wall provided the optical depth in the polar region is low, though this is likely only at lower accretion rates. In

both cases, it is required that the TDE candidates must be observed within the jet beaming angle, because the luminosity would be significantly lower for more inclined observers (Fig. 6).

4.2.2 Ultraluminous X-ray sources

ULXs are objects emitting isotropic equivalent luminosities in excess of 10^{39} erg s^{-1} (e.g. Miller, Fabian & Miller 2004). The critical number corresponds roughly to the Eddington luminosity for a $10\,M_\odot$ central source. A standard thin disc around a $10\,M_\odot$ BH, accreting at a sub-Eddington rate, cannot produce the luminosity observed in ULXs, so one possibility is that the accreting compact objects are intermediate-mass BHs. However, if the emitted radiation is beamed into a relatively narrow solid angle, the observed luminosity can easily exceed the Eddington value for observers located in favourable directions, even though the total emission may still be subcritical. In this scenario, ULXs are normal $\sim 10\,M_\odot$ BHs (King 2009).

Our study supports the latter picture since we find very strong beaming of radiation in geometrically thick discs. The particular systems we studied have very high and extreme accretion rates. In these flows, the funnel region is optically thick and radiative energy is efficiently converted into kinetic energy of the outflowing, collimated gas. Whether or not this kinetic energy can be dissipated in shocks to produce radiation and whether the resulting spectrum would match observations of ULXs is uncertain.

However, another regime of supercritical accretion may be more applicable to ULXs. For not-so-extreme accretion rates, say $\dot{M} \sim 10\,\dot{M}_{\rm Edd}$, the polar region is optically thin and conversion of radiative to kinetic energy is not efficient. It is then possible to observe directly the radiation emitted inside the funnel. Although the beaming may be less strong, it can still magnify the observed luminosity and cause a stellar-mass BH source accreting at a moderately supercritical rate to match the isotropic-equivalent luminosities observed in ULXs. Detailed modelling of the observational properties of such systems was done by Kawashima et al. (2012) using simulation data corresponding to a mildly supercritical ($\sim 10\,\dot{M}_{\rm Edd}$) accretion flow on a $10\,M_\odot$ BH. The simulation was done with a Newtonian radiation MHD code. The authors showed that Comptonization in the polar region significantly hardens the original photon spectrum.

We have estimated the beaming factor, defined as the ratio of the observed (isotropic equivalent) to the real (integrated over the sphere) luminosities, and find (Fig. 6) that it significantly decreases with increasing polar angle. Therefore, one should expect that, for the same BH mass and accretion rate, the distribution of ULX luminosities will be sensitive to the orientation on the sky.

4.2.3 SS433

SS433 is the first microquasar to be discovered. It is an eclipsing X-ray binary system in which the compact primary object is most likely a BH with $M_{\rm BH} \approx 10\,M_\odot$ (Grindlay et al. 1984). The wind of the companion star feeds the central object at an extremely high rate. The measured disc wind outflow rates are $\dot{M} = 10^{-5}$–$10^{-4}\,M_\odot\,{\rm yr}^{-1}$ (Shklovsky 1981) which suggest that the accretion rate on to the compact object is supercritical. A direct measurement of the accretion $\dot{M}$ is, however, impossible because the innermost regions of the disc are obscured. SS433 shows powerful jets precessing with a period of 162 d and sweeping twin cones with half-angle $20°$. The jets are loaded with baryons and move

at a velocity of $0.26c$ (Margon 1984; Fabrika 2004). The corresponding kinetic power dominates the jet energy budget and equals $10^{39.3}$–$10^{39.7}$ erg s^{-1} (Marshall et al. in preparation).

The fact that the jets are precessing suggests that the BH spin is non-zero and that there is a misalignment between the angular momentum of the binary and the BH spin axis. These conditions have to be satisfied for Lense–Thirring precession (Bardeen & Petterson 1975) to occur. If the BH is spinning, then it seems reasonable to assume that the observed jets are powered by the BH rotational energy via a strong magnetic field. However, the origin of the baryons in the jet is then problem since the magnetic field lines will screen the baryons in the disc from the jet region. It has been suggested that the jets are initially leptonic, but they then acquire baryons when they collide either with the thick accretion disc itself or the disc wind.

We propose another explanation for the baryon-loaded jets in SS433. The mass supply rate on the compact object most likely corresponds to a supercritical accretion. At such high accretion rates, an optically thick and geometrically thick disc will form and, as shown in this work, radiation moves into the polar region, pushing gas along with it and making the funnel optically thick. The radiation then escapes up the funnel and accelerates the gas, thus converting a good fraction of the total energy flux into jet kinetic energy. Once such a radiatively driven jet crosses the funnel photosphere, it is baryon-loaded, kinetically dominated and collimated.

These features in our simulations are consistent with observations of the jets in SS433. The density-averaged gas velocity in our simulated jets is of the order of 0.2–$0.3c$ (bottom panel of Fig. 3), which is in excellent agreement with the velocity observed in SS433. For a $10\,M_\odot$ BH accreting at $100\,\dot{M}_{\rm Edd}$, the jet power we expect based on the simulations is roughly $0.01\,\dot{M}c^2 \approx 2 \times 10^{40}$ erg s^{-1}. This is more than adequate to explain the observed kinetic luminosity of the jets in SS433.

The non-zero BH spin and misalignment between the orbital and BH spin axes, both of which are required for jet precessions, suggest that additional effects over and above simple radiative acceleration might be operating. The small observed opening angle of the jet in SS433 ($1°$–$2°$), is not consistent with the jets seen in the simulations, which have opening angles of the order of $10°$–$15°$ (Fig. 6). Perhaps there are magnetic effects on top of the radiative processes we have discussed, which cause strong collimation.

REFERENCES

Abramowicz M. A., Piran T., 1980, ApJ, 241, L7
Abramowicz M., Jaroszynski M., Sikora M., 1978, A&A, 63, 221

Abramowicz M. A., Ellis G. F. R., Lanza A., 1990, ApJ, 361, 470

Arcavi I. et al., 2014, ApJ, 793, 38

Bardeen J. M., Petterson J. A., 1975, ApJ, 195, L65

Berger E., Zauderer A., Pooley G. G., Soderberg A. M., Sari R., Brunthaler A., Bietenholz M. F., 2012, ApJ, 748, 36

Blandford R. D., Znajek R. L., 1977, MNRAS, 179, 433 (BZ)

Bloom J. S. et al., 2011, Science, 333, 203

Bonnerot C., Rossi E. M., Lodato G., Price D. J., 2015, preprint (arXiv:1501.04635)

Burrows D. N. et al., 2011, Nature, 476, 421

Chornock R. et al., 2014, ApJ, 780, 44

Evans C. R., Kochanek C. S., 1989, ApJ, 346, L13

Fabrika S., 2004, Astrophy. Space Phys. Rev., 12, 1

Fishbone L. G., Moncrief V., 1976, ApJ, 207, 962

Fragile P. C., Olejar A., Anninos P., 2014, ApJ, 796, 22

Gezari S. et al., 2012, Nature, 485, 217

Grindlay J. E., Band D., Seward F., Leahy D., Weisskopf M. C., Marshall F. E., 1984, ApJ, 277, 286

Igumenshchev I. V., Narayan R., Abramowicz M. A., 2003, ApJ, 592, 1042

Jaroszynski M., Abramowicz M. A., Paczynski B., 1980, Acta Astron., 30, 1

Jiang Y.-F., Stone J. M., Davis S. W., 2014, ApJ, 796, 106

Kawashima T., Ohsuga K., Mineshige S., Yoshida T., Heinzeller D., Matsumoto R., 2012, ApJ, 752, 18

Kelley L. Z., Tchekhovskoy A., Narayan R., 2014, MNRAS, 445, 3919

King A. R., 2009, MNRAS, 393, L41

Kozlowski M., Jaroszynski M., Abramowicz M. A., 1978, A&A, 63, 209

Krolik J. H., Piran T., 2012, ApJ, 749, 92

Lasota J.-P., Gourgoulhon E., Abramowicz M., Tchekhovskoy A., Narayan R., 2014, Phys. Rev. D, 89, 024041

Levermore C. D., 1984, J. Quant. Spectrosc. Radiat. Transfer., 31, 149

McKinney J. C., Tchekhovskoy A., Blandford R. D., 2012, MNRAS, 423, 3083

McKinney J. C., Tchekhovskoy A., Sadowski A., Narayan R., 2014, MNRAS, 441, 3177

Madau P., 1988, ApJ, 327, 116

Margon B., 1984, ARA&A, 22, 507

Miller J. M., Fabian A. C., Miller M. C., 2004, ApJ, 614, L117

Narayan R., Nityananda R., Wiita P. J., 1983, MNRAS, 205, 1103

Narayan R., Igumenshchev I. V., Abramowicz M. A., 2003, PASJ, 55, L69

Ohsuga K., Mineshige S., 2007, ApJ, 670, 1283

Ohsuga K., Mineshige S., 2011, ApJ, 736, 2

Ohsuga K., Mori M., Nakamoto T., Mineshige S., 2005, ApJ, 628, 368

Ohsuga K., Mineshige S., Mori M., Yoshiaki K., 2009, PASJ, 61, L7

Paczyński B., Wiita P. J., 1980, A&A, 88, 23

Penna R. F., Narayan R., Sądowski A., 2013a, MNRAS, 436, 3741

Penna R. F., Kulkarni A., Narayan R., 2013b, A&A, 559, A116

Piran T., 1982, ApJ, 257, L23

Rees M. J., 1988, Nature, 333, 523

Shiokawa H., Krolik J. H., Cheng R. M., Piran T., Noble S. C., 2015, AJ, 804, 85

Shklovsky I. S., 1981, Astron. Zh., 58, 554

Sikora M., 1981, MNRAS, 196, 257

Sikora M., Wilson D. B., 1981, MNRAS, 197, 529

Sironi L., Petropoulou M., Giannios D., 2015, MNRAS, 450, 183

Sądowski A., Narayan R., Tchekhovskoy A., Zhu Y., 2013a, MNRAS, 429, 3533

Sądowski A., Narayan R., Penna R., Zhu Y., 2013b, MNRAS, 436, 3856

Sądowski A., Narayan R., McKinney J. C., Tchekhovskoy A., 2014, MNRAS, 439, 503

Sądowski A., Narayan R., Tchekhovskoy A., Abarca D., Zhu Y., McKinney J. C., 2015, MNRAS, 447, 49

Takahashi H. R., Ohsuga K., 2015, PASJ, 160

Takeuchi S., Ohsuga K., Mineshige S., 2010, PASJ, 62, L43

Tchekhovskoy A., McKinney J. C., 2012, MNRAS, 423, L55

Tchekhovskoy A., Narayan R., McKinney J. C., 2010, New Astron., 15, 749

Tchekhovskoy A., Narayan R., McKinney J. C., 2011, MNRAS, 418, L79

Tchekhovskoy A., Metzger B. D., Giannios D., Kelley L. Z., 2014, MNRAS, 437, 2744

This paper has been typeset from a TEX/LATEX file prepared by the author.